SCIENCE CHINA
Technological Sciences

•Article•

https://doi.org/10.1007/s11431-023-2529-3

A novel approach towards the selection of regenerators for optimal Stirling engine performance based on energy and exergy analyses

YU MinJie, ZHANG MingHui, XU Lei, CUI HaiChuan, LIU ZhiChun & LIU Wei*

School of Energy and Power Engineering, Huazhong University of Science and Technology, Wuhan 430074, China

Received August 2, 2023; accepted October 17, 2023; published online December 15, 2023

Regenerators play a vital role in enhancing the overall performance of Stirling engines. Hence, this paper performed an energy and exergy analysis to elucidate the significance of regenerator characteristics concerning system performance, contributing to the optimal regenerator's design and selection. The relationship between regenerator structure, regenerator exergy destruction, and output power, thermal efficiency, and exergy efficiency for Stirling engines was established by integrating the thermal model of Stirling engines with a mathematical model of regenerators. In contrast to cross-flow and parallel-flow regenerators, a novel concept of inclined-flow regenerators, featuring a matrix surface inclined in the direction of gas flow, was developed to achieve higher and more balanced engine output power and energy utilization efficiency. A comprehensive investigation was conducted into the effects of matrix structure types and regenerator geometries on the performance of both regenerators and engines. The results reveal that, following structural optimization, Stirling engines equipped with the inclined-flow regenerator demonstrate a substantial 16.6%, 38.3%, and 37.2% increase in power output, thermal efficiency, and exergy efficiency, respectively, compared to those equipped with cross-flow regenerators. In contrast, when compared to engines fitted with parallel-flow regenerators, they experience a 13.5% reduction in power output but achieve remarkable enhancements of 45.4% and 36.7% in thermal and exergy efficiency, respectively. This study introduces new insights into selecting regenerator structures for enhancing the output performance of Stirling engines.

Stirling engine, inclined-flow regenerator, adiabatic model, exergy analysis

Citation: Yu M J, Zhang M H, Xu L, et al. A novel approach towards the selection of regenerators for optimal Stirling engine performance based on energy and exergy analyses. Sci China Tech Sci, 2023, 66, https://doi.org/10.1007/s11431-023-2529-3

1 Introduction

Clean and renewable energy sources such as solar, biomass, and geothermal energy have garnered increasing attention [1]. Efficiently harnessing these energy sources has emerged as a critical research focus [2]. Stirling engines, as external combustion engines, offer the versatility to harness a wide range of external thermal energy sources. They possess several advantageous characteristics such as high theoretical thermal efficiency, low emissions, and quiet operation. Consequently, Stirling engines hold significant promise in the integration of renewable energy sources [3,4].

Stirling engines are typically composed of two working spaces (compression and expansion chambers), three heat exchangers (heater, regenerator, and cooler), two pistons, and various auxiliary components. Among these components, the regenerator plays a crucial role in ensuring the efficient operation of Stirling engines [5]. Positioned between the heater and cooler, the regenerator matrix alternately absorbs and releases heat as the working gas reciprocates through it. In essence, the regenerator functions like a thermal sponge, significantly enhancing the utilization of heat absorbed by the heater, reducing the size requirements of the heater and cooler, and ultimately improving the thermal efficiency of the system [6]. Currently, the most commonly used regenerators can be broadly categorized as

*Corresponding author (email: w_liu@hust.edu.cn)

cross-flow [7,8] and parallel-flow regenerators [9,10] based on the flow pattern of the working gas in the matrix. In the cross-flow regenerator, the gas flows perpendicular to the matrix surface, leading to strong gas-matrix interaction. This results in high heat transfer rates but also imposes significant flow resistance. In contrast, parallel-flow regenerators feature gas flow parallel to the matrix surface, resulting in reduced flow losses but also a notable decrease in thermal performance compared to cross-flow regenerators. Excessive pressure drop or insufficient heat transfer performance in a regenerator can significantly undermine its overall effectiveness, consequently reducing the power output and thermal efficiency of Stirling engines [11]. To enhance the overall flow and thermal performance, exploring the development of an inclined-flow regenerator, which incorporates matrix structures and gas flow patterns intermediate to those of cross-flow and parallel-flow regenerators, represents a logical proposition.

Research into regenerators can be carried out at two levels: component level and engine level. Previous studies in the existing literature primarily concentrated on analyzing the flow resistance and heat transfer characteristics of regenerators at the component level, without delving into how these regenerator traits impact the heat-to-work conversion performance of Stirling engines [12–19]. Concerning research at the engine level, some previous work explored phenomena related to temperature differences between the two sides of the regenerator [20,21] and between the working gas and the matrix [22] and expounded their influence on engine performance. Others introduced the analysis of irreversible losses in regenerators into theoretical engine models, estimating regenerator heat and power losses using empirical correlations or classical thermodynamic derivations [23–29]. However, these studies did not encompass the effects of different matrix structures and various geometric parameters of regenerators on engine performance. To date, only a limited number of numerical [30] and experimental [31] work have been conducted to detect the power output and thermal efficiency of Stirling engines under different regenerator geometric parameters, such as the wire diameter and porosity. These studies have been crucial in revealing the relationship between regenerator geometric parameters and engine performance, guiding regenerator optimization. Nevertheless, the effects of the regenerator matrix types and global geometric parameters, such as the regenerator volume and length, have not been investigated in detail, and the mechanism through which the regenerators with various geometric dimensions influence the engine performance remains unclear. Hence, to comprehend the mechanism by which regenerator structures affect engine performance, it is imperative to establish the relationship between regenerator structures, the flow and heat transfer characteristics of regenerators, and the heat-to-work conversion performance of engines. A feasible approach for achieving this is to integrate the performance analysis of both the regenerator and the engine by combining the mathematical model of regenerators with an engine model.

In recent decades, numerous thermodynamic models have been developed to analyze and predict the performance of Stirling engines. These engine models can be categorized into empirical [32,33], analytical [34,35], and numerical methods. The first two types of models tremendously simplify the real Stirling engine and do not take complicated and detailed engine parameters into account, thus offering low accuracy. Numerical models can be further concretely classified into second-order [36–41], third-order [42–44], and multi-dimensional computational fluid dynamics (CFD) [45–48] analyses. Third-order and multi-dimensional CFD models discretize the Stirling engine into multiple nodes or control volumes in one- and multi-dimensional spaces, respectively, and solve the governing equations for each node or control volume [49]. Compared with other models, they can capture more detailed operating information about engines and offer high precision but require relatively more computational resources. In contrast, second-order methods include only the five most critical components, significantly reducing the computational cost. Simultaneously, these second-order models offer acceptable accuracy, though slightly lower than that of third-order and multi-dimensional CFD models. Consequently, second-order methods have been widely employed in the performance analysis of Stirling engines, with the adiabatic model and its improved versions being the most commonly used among researchers. In this study, we adopted the ideal adiabatic model to predict the performance of regenerators and engines in combination with the regenerator model.

Considering the aforementioned points, this study is devoted to performing a new energy and exergy analysis of Stirling engines with the detailed loss effects of regenerators, by combining the adiabatic model with a regenerator mathematical model. To improve the overall performance of Stirling engines, a new type of inclined-flow regenerator, with the matrix surface inclined to the gas flow direction, was developed to strike a well-balanced compromise between the flow and heat transfer characteristics of cross-flow and parallel-flow regenerators. Four criteria, including the total exergy destruction rate, actual power output, thermal efficiency, and exergy efficiency, were selected to evaluate the performance of the regenerator and engine. The relationship between the regenerator geometry, regenerator exergy destruction, actual power output, and energy utilization efficiency of engines was established, and the effects of matrix structure types and geometric parameters of regenerators on the performance of both regenerators and Stirling engines were thoroughly investigated and analyzed. The primary innovations of the present study can be sum-

marized as follows: (1) the development of a new concept of inclined-flow regenerators; (2) the introduction of a novel approach to regenerator structure design and selection, aiming to enhance engine performance from a system perspective. These findings offer valuable guidelines for achieving higher performance in Stirling engines through the appropriate selection of regenerators.

2 Ideal adiabatic model of Stirling engines

In the ideal adiabatic model, the Stirling engine is divided into five distinct parts, as visually represented in Figure 1. In this diagram, the single subscripts "*c*", "*k*", "*r*", "*h*", and "*e*" represent the compression chamber, cooler, regenerator, heater, and expansion chamber, respectively, and the double subscripts "*ck*", "*kr*", "*rh*", and "*he*" denote the interfaces between each pair of adjacent parts. Each part is treated as an individual control volume, where the physical field is assumed to be uniformly distributed. To obtain the equation system for the adiabatic model, some assumptions are made as follows [36,37].

(1) The working gas used in the engine (helium) is considered as the ideal gas.

(2) The pressure of the gas is uniform in the whole engine.

(3) The gas in the compression and expansion chambers is adiabatic.

(4) The temperature of the gas in the heater and cooler is kept constant.

Based on the aforementioned assumptions, the equation system of the adiabatic model can be derived from the conservation equations of mass and energy and the ideal gas equation of state for each control volume, as detailed in Table 1. This equation system comprises ordinary differential equations, mass flow equations at the interfaces of adjoining sections, and boundary temperature equations by conditional judgment. In these equations, the differential symbol $d \equiv d/d\theta$, where θ is the crank angle.

3 Mathematical model of regenerators

3.1 Regenerator geometries

The typical configuration for a regenerator employed in Stirling engines is that of an annular cylinder, as illustrated in Figure 2. This regenerator is characterized by inner and outer diameters denoted as d_1 and d_2, respectively, and a length represented by L. For ease of analysis, the regenerator is treated as an isotropic porous medium model with a porosity of φ. Additionally, as the regenerator reaches a steady operational state, the variation in the physical field along the radial direction is significantly smaller than that along the axial direction. Hence, this three-dimensional regenerator can be further simplified into a one-dimensional model, considering only the axial variations in physical fields. In practical Stirling engine manufacturing, cost-effectiveness and spatial constraints demand precise alignment of component dimensions. Consequently, overall geometric parameters, including regenerator volume, are often constrained. To better emulate real-world scenarios, we assumed a constant total volume when determining local regenerator geometric parameters. As a result, with the regenerator length specified, the cross-sectional area of the regenerator can be calculated as

$$A = \frac{V}{L}. \tag{1}$$

3.2 Governing equations

During the regenerative process, significant spatial and

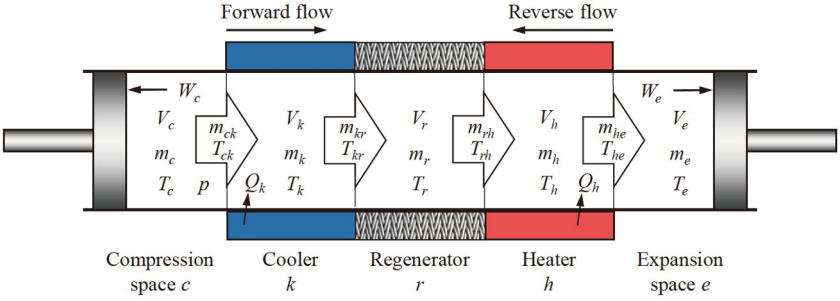

Figure 1 (Color online) Five parts of Stirling engines in the ideal adiabatic model.

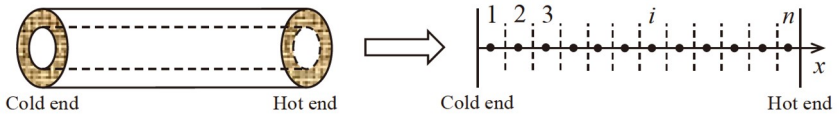

Figure 2 (Color online) Schematic of the regenerator and its simplified model.

Table 1 Equation system of the ideal adiabatic model

Equation system	Ideal adiabatic model
$V_e = \frac{V_{se}}{2}\left(1-\cos\left(\theta+\theta_0\right)\right)+V_{ed}$	Volume variation
$V_c = \frac{V_{se}}{2}(1+\cos\theta)+\frac{V_{sc}}{2}\left(1-\cos\left(\theta+\theta_0-\psi\right)\right)+V_{cd}$	
$p = \frac{RM}{\frac{V_c}{T_c}+\frac{V_k}{T_k}+\frac{V_r}{T_r}+\frac{V_h}{T_h}+\frac{V_e}{T_e}}$	Pressure
$\mathrm{d}p = \frac{-\gamma p\left(\frac{\mathrm{d}V_c}{T_{ck}}+\frac{\mathrm{d}V_e}{T_{he}}\right)}{\left[\frac{V_c}{T_{ck}}+\gamma\left(\frac{V_k}{T_k}+\frac{V_r}{T_r}+\frac{V_h}{T_h}\right)+\frac{V_e}{T_{he}}\right]}$	Pressure variation
$m_i = \frac{pV_i}{RT_i}, i = c,k,r,h,e$	Mass
$\mathrm{d}m_i = m_i\frac{\mathrm{d}p}{p}, i = k,r,h$	
$\mathrm{d}m_c = \frac{p\mathrm{d}V_c+\frac{1}{\gamma}V_c\mathrm{d}p}{RT_{ck}}$	Mass variation
$\mathrm{d}m_e = \frac{p\mathrm{d}V_e+\frac{1}{\gamma}V_e\mathrm{d}p}{RT_{he}}$	
$\dot{m}_{ck} = -dm_c$	
$\dot{m}_{kr} = \dot{m}_{ck}-dm_k$	Mass flow rate at the interface
$\dot{m}_{rh} = \dot{m}_{kr}-dm_r$	
$\dot{m}_{he} = \dot{m}_{rh}-dm_h$	
if $\dot{m}_{ck} > 0$, then $T_{ck} = T_c$, else, $T_{ck} = T_k$	Temperature at the interface
if $\dot{m}_{he} > 0$, then $T_{he} = T_h$, else, $T_{he} = T_e$	
$\mathrm{d}T_c = T_c\left(\frac{\mathrm{d}p}{p}+\frac{\mathrm{d}V_c}{V_c}-\frac{\mathrm{d}m_c}{m_c}\right)$	Temperature variation
$\mathrm{d}T_e = T_e\left(\frac{\mathrm{d}p}{p}+\frac{\mathrm{d}V_e}{V_e}-\frac{\mathrm{d}m_e}{m_e}\right)$	
$\mathrm{d}Q_k = \frac{c_vV_k\mathrm{d}p}{R}+c_p\left(\dot{m}_{kr}T_{kr}-\dot{m}_{ck}T_{ck}\right)$	Heat output of the cooler
$\mathrm{d}Q_h = \frac{c_vV_h\mathrm{d}p}{R}+c_p\left(\dot{m}_{he}T_{he}-\dot{m}_{rh}T_{rh}\right)$	Heat input of the heater
$\mathrm{d}Q_r = \frac{c_vV_r\mathrm{d}p}{R}+c_p\left(\dot{m}_{rh}T_{rh}-\dot{m}_{kr}T_{kr}\right)$	Heat transfer of the regenerator
$\mathrm{d}W_c = p\mathrm{d}V_c$	Work in the compression process
$\mathrm{d}W_e = p\mathrm{d}V_e$	Work in the expansion process

temporal variations in gas pressure, temperature, and solid temperature take place within the regenerator. Consequently, this study incorporates the gas's compressibility by employing the ideal gas state equation to ascertain gas density. Gas viscosity, thermal conductivity, and matrix thermal conductivity are considered as functions of temperature, while all other physical properties remain constant. Besides, the effects of all the body forces and external heat losses are neglected. Under these assumptions, the gas flow and heat transfer in the regenerator are characterized as one-dimensional unsteady viscous compressible flow and gas-solid coupling heat transfer. Consequently, the governing equa-

tions describing the conservation of mass, momentum, and energy in the regenerator can be expressed as follows [50,51].

The mass conservation equation:

$$\frac{\partial(\varphi\rho_f)}{\partial t}+\frac{\partial(\rho_f u)}{\partial x}=0, \tag{2}$$

where ρ_f and u denote the density and velocity of the gas, respectively; φ is the porosity of the regenerator matrix; and t and x represent the time and the axial direction of the regenerator, respectively.

The momentum conservation equation:

$$\left(\frac{1}{\varphi}\frac{\partial(\rho_f u)}{\partial t}+\frac{1}{\varphi^2}\frac{\partial(\rho_f uu)}{\partial x}\right)$$
$$=-\frac{\partial p}{\partial x}+\frac{\mu_f}{\varphi}\frac{\partial^2 u}{\partial x^2}-\left(\frac{\mu_f}{K}u+\frac{C_2\rho_f}{2}|u|u\right), \tag{3}$$

where p and μ are the pressure and viscosity of the gas, respectively; and K and C_2 represent the permeability and inertial resistance coefficient of the matrix, respectively.

The energy conservation equation of the gas:

$$c_{p,f}\left(\varphi\frac{\partial(\rho_f T_f)}{\partial t}+\frac{\partial(\rho_f uT_f)}{\partial x}\right)$$
$$=\varphi k_f\frac{\partial^2 T_f}{\partial x^2}-\frac{\partial(up)}{\partial x}+h\alpha_r\left(T_s-T_f\right). \tag{4}$$

The energy conservation equation of the matrix solid:

$$\rho_s c_s(1-\varphi)\frac{\partial T_s}{\partial t}=(1-\varphi)k_s\frac{\partial^2 T_s}{\partial x^2}+h\alpha_r\left(T_f-T_s\right), \tag{5}$$

where T_f, $c_{p,f}$, and k_f denote the temperature, specific heat at constant pressure, and thermal conductivity of the gas, respectively; T_s, c_s, and k_s denote the temperature, specific heat, and effective thermal conductivity of the matrix, respectively; h is the heat transfer coefficient between the gas and the matrix; and α_r is the specific surface area of the matrix, which is calculated by

$$\alpha_r=\frac{4\varphi}{d_h}, \tag{6}$$

where d_h is the hydraulic diameter of the regenerator matrix, which can be determined as

$$d_h=\frac{4\varphi V}{A_s}, \tag{7}$$

where A_s is the total surface area of the regenerator matrix.

In governing eqs. (2)–(5), five unknown variables p_f, u, p, T_f, and T_s are included. To obtain a closed equation system, the ideal gas equation of state is introduced to solve the density profile of the gas in the regenerator:

$$p=R\rho_f T_f. \tag{8}$$

3.3 Concept of inclined-flow regenerators

Figure 3 depicts the schematic representation of different regenerator matrix structure types and their corresponding gas-matrix interaction patterns. As illustrated in Figure 3(a) and (b), the cross-flow regenerator involves a gas flow direction perpendicular to the matrix surface, causing the gas to flow around the matrix surface. In contrast, for the parallel-flow regenerator, the gas flows parallel to the matrix surface, along the extended surface of the matrix. However, in Figure 3(c), the matrix surface of the inclined-flow regenerator is tilted in the direction of the gas flow, so that a moderate interaction between the gas and matrix is obtained, which will be expected to bring about a well-balanced flow and heat transfer characteristic for the inclined-flow regenerator. For quantitatively analyzing and comparing the comprehensive performance of the three types of regenerators, the resistance coefficient f and the Nusselt number Nu of the inclined-flow regenerator are assumed to maintain a linear relationship with those of the cross-flow and parallel-flow regenerators, as presented below.

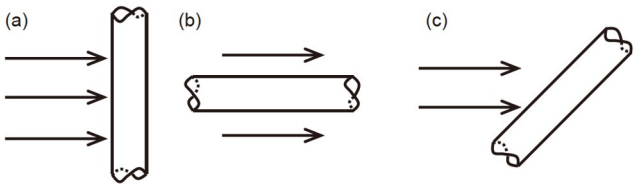

Figure 3 Different matrix structure types of regenerators and the corresponding flow patterns of the gas inside them. (a) Cross-flow regenerator; (b) parallel-flow regenerator; (c) inclined-flow regenerator.

$$f=f_p+\zeta(f_c-f_p), \tag{9}$$

$$Nu=Nu_p+\zeta\left(Nu_c-Nu_p\right), \tag{10}$$

where f_c and Nu_c denote the resistance coefficient and Nusselt number for the cross-flow regenerator, and f_p and Nu_p denote the resistance coefficient and Nusselt number for the parallel-flow regenerator. ζ is the matrix structure coefficient, which determines the thermo-hydraulic characteristic level of the regenerator, and its value range is $0\leqslant\zeta\leqslant 1$. Specially, when the ζ equals 0 or 1, it signifies the characteristic levels of the parallel-flow regenerator and cross-flow regenerator, respectively. For values of ζ between 0 and 1, a higher ζ means that the matrix structure, as well as the flow and thermal characteristics of the inclined-flow regenerator, closely resemble those of the cross-flow regenerator. Conversely, a lower value of ζ implies a greater similarity to the parallel-flow regenerator.

Two crucial points warrant clarification. First, the wire-shaped matrix geometry depicted in Figure 3 serves to visually illustrate the gas-matrix interaction patterns inside the three types of regenerators, but it is not the unique structure for each type of regenerator matrix. In actuality, any matrix featuring a surface perpendicular, parallel, or inclined to the gas flow direction can be categorized into these three types of regenerators. Herein, no specific inclined-flow

regenerator matrix is proposed. Further studies are required to design the inclined-flow regenerator with specific matrix structures. Second, altering the regenerator matrix structure usually brings about a synergistic variation of flow resistance and heat transfer characteristics. To reflect this phenomenon, a linear relationship between the thermo-hydraulic performance of the inclined-flow regenerator and those of the cross-flow and parallel-flow regenerators is assumed. However, it is not the characteristic of a specific regenerator matrix but rather reflects the desired behavior for an inclined-flow regenerator. In further studies, verification and structure modification will be undertaken for the specific inclined-flow regenerator matrix to ensure that it aligns closely with the intended thermo-hydraulic characteristics.

In this study, the classical woven screen regenerator and circular micro-channel regenerator are employed to represent the cross-flow regenerator and parallel-flow regenerator, respectively, whose resistance coefficient and Nusselt number are given as follows.

Woven screen regenerators [52]:

$$f_c = \frac{175}{Re_h} + 1.6, \tag{11}$$

$$Nu_c = 0.33 Re_h^{0.67}. \tag{12}$$

Circular micro-channel regenerators [53]:

$$f_p = \frac{64}{Re_h}, \tag{13}$$

$$Nu_p = 1.143 Re_h^{0.2488}, \tag{14}$$

where Re_h is the hydraulic Reynolds number, which can be calculated by

$$Re_h = \frac{u d_h \rho_f}{\mu}. \tag{15}$$

Substituting eqs. (11) and (13) into eq. (9), the resistance coefficient of the inclined-flow regenerator can be obtained as

$$f = \frac{111\zeta + 64}{Re_h} + 1.6\zeta. \tag{16}$$

Additionally, according to ref. [54], the following correlation is given:

$$f = \frac{2d_h^2}{KRe_h} + C_2 d_h. \tag{17}$$

By comparing eqs. (16) and (17), the permeability and inertial resistance coefficient of the regenerator are gained as

$$K = \frac{2d_h^2}{111\zeta + 64}, \tag{18}$$

$$C_2 = \frac{1.6\zeta}{d_h}. \tag{19}$$

Similarly, substituting eqs. (12) and (14) into eq. (10), the Nusselt number of the inclined-flow regenerator can be determined as

$$Nu = (1.143 - 1.143\zeta) Re_h^{0.2488} + 0.33\zeta Re_h^{0.67}. \tag{20}$$

Hence, the heat transfer coefficient between the gas and matrix in the regenerator is calculated as

$$h = (1.143 - 1.143\zeta) k_f d_h^{-0.7512} \left(\frac{u\rho_f}{\mu}\right)^{0.2488} + 0.33\zeta k_f d_h^{-0.33} \left(\frac{u\rho_f}{\mu}\right)^{0.67}. \tag{21}$$

4 Performance criteria

4.1 Regenerator performance

Herein, the total exergy destruction rate generated by the factors of inefficiency in the regenerative process is adopted to characterize the regenerator performance. A higher total exergy destruction rate signifies lower regenerator performance and exerts a more substantial negative influence on engine performance. The total exergy destruction in the regenerator can be expressed as [51]

$$\dot{E}_{xd,tot} = \dot{E}_{xd,ht} + \dot{E}_{xd,fr} + \dot{E}_{xd,gc} + \dot{E}_{xd,sc}, \tag{22}$$

where the four terms in the right side of the equation are the exergy destruction rate caused by the gas-solid heat transfer with a finite temperature difference, gas flow resistance, and axial heat conduction in the gas and matrix, respectively, which can be determined by the following equations.

The entropy generation resulted from the gas-solid heat transfer with a finite temperature difference in a single cycle is calculated as [55]

$$\begin{aligned} S_{ht} &= \int_0^\tau Q\left(\frac{1}{T_s} - \frac{1}{T_f}\right)\mathrm{d}t \\ &= \int_0^\tau \int_0^L h\Delta T\left(\frac{1}{T_s} - \frac{1}{T_f}\right)\alpha_r A\mathrm{d}x\mathrm{d}t \\ &= \int_0^\tau \int_0^L h\alpha_r \frac{(\Delta T)^2}{T_s T_f} A\mathrm{d}x\mathrm{d}t, \end{aligned} \tag{23}$$

where Q is the heat flux at the gas-solid interface, ΔT is the local temperature difference between the gas and the matrix, and τ is the cycle length of the Stirling engine that is defined as $\tau = 60/n$, where n is the engine speed.

Based on eq. (23), the exergy destruction rate due to the gas-solid heat transfer with a finite temperature difference can be obtained as

$$\dot{E}_{xd,ht} = T_0 S_{ht} \frac{n}{60}, \tag{24}$$

where T_0 denotes the ambient temperature and is set as 288 K in this study.

The exergy destruction caused by the flow resistance in a single cycle is defined as [51]

$$E_{xd,fr}=\int_0^{\tau}\int_0^{L}\left|-\frac{\mathrm{d}p}{\mathrm{d}x}u\right|A\mathrm{d}x\mathrm{d}t. \tag{25}$$

Therefore, the exergy destruction rate due to the flow resistance in the regenerator is determined as

$$\dot{E}_{xd,fr}=E_{xd,fr}\frac{n}{60}. \tag{26}$$

The entropy generation resulted from the axial heat conduction in the gas and matrix in a single cycle is respectively given as [51]

$$S_{gc}=\int_0^{\tau}\int_0^{L}\frac{\varphi k_f}{T_f^2}\left(\frac{\mathrm{d}T_f}{\mathrm{d}x}\right)^2A\mathrm{d}x\mathrm{d}t, \tag{27}$$

$$S_{sc}=\int_0^{\tau}\int_0^{L}\frac{(1-\varphi)k_s}{T_s^2}\left(\frac{\mathrm{d}T_s}{\mathrm{d}x}\right)^2A\mathrm{d}x\mathrm{d}t. \tag{28}$$

Consequently, the exergy destruction rate due to the axial heat conduction of the gas and matrix can be calculated as

$$\dot{E}_{xd,gc}=T_0S_{gc}\frac{n}{60}, \tag{29}$$

$$\dot{E}_{xd,sc}=T_0S_{sc}\frac{n}{60}. \tag{30}$$

4.2 Stirling engine performance

To quantitatively evaluate the overall performance of Stirling engines, the actual power output, thermal efficiency, and exergy efficiency are selected as the criteria in this work. Based on the ideal adiabatic model, the ideal net work output and power output are respectively obtained as

$$W_i=\int_{t=0}^{t=\tau}p\mathrm{d}V_e+\int_{t=0}^{t=\tau}p\mathrm{d}V_c, \tag{31}$$

$$P_i=W_i\frac{n}{60}. \tag{32}$$

Since the effect of the regenerator is the focus of this study, other irreversible losses in Stirling engines are ignored. As a result, the actual power output of the engine is calculated as

$$P_s=P_i-\dot{E}_{xd,fr}. \tag{33}$$

Besides, according to the ideal adiabatic model, the ideal heat input and heat input rate are respectively given as

$$Q_h=\int_{t=0}^{t=\tau}\mathrm{d}Q_h, \tag{34}$$

$$\dot{Q}_h=Q_h\frac{n}{60}. \tag{35}$$

The thermal efficiency of the engine can be calculated as

$$\eta_{th}=\frac{P_s}{\dot{Q}_h+\left(\dot{E}_{xd,ht}+\dot{E}_{xd,gc}+\dot{E}_{xd,sc}\right)/\left(1-T_0/\left(\frac{T_h+T_k}{2}\right)\right)}. \tag{36}$$

The exergy efficiency of Stirling engines is the ratio of the actual power output to the actual exergy input rate. Thereby, the exergy efficiency of the engine is determined as [56,57]

$$\eta_{ex}=\frac{P_s}{\dot{Q}_h\left(1-\frac{T_0}{T_h}\right)+\dot{E}_{xd,ht}+\dot{E}_{xd,gc}+\dot{E}_{xd,sc}}. \tag{37}$$

5 Solution methods

5.1 Initial and boundary conditions

The solution to the ideal adiabatic model of Stirling engines is an initial value problem. The equation systems can be solved by giving appropriate initial conditions according to the geometric and operating conditions of engines, including those related to the regenerator. In this study, certain assumptions have been made regarding the temperatures of the working gas in the heater and cooler, which are considered to be equivalent to those of the heat source and heat sink, respectively. Additionally, the regenerator temperature is presumed to match the logarithmic mean temperature of the heater and cooler. Furthermore, the initial gas temperature within the compression chamber and expansion chamber is set equal to the temperature of the heat sink and heat source, respectively. Lastly, the initial pressure inside the engine is configured to align with the charge pressure.

The mathematical model of the regenerator necessitates the specification of both boundary and initial conditions for a comprehensive solution. Herein, the instantaneous mass flow rate at the cold end of the regenerator and instantaneous pressure of the engine, both derived from the ideal adiabatic model and detailed in Table 1, are set as the cold end and hot end boundary conditions of the regenerator model, respectively, as expressed in eqs. (38) and (39). Additionally, when the gas enters the regenerator from the cold end, the temperature of the heat sink is applied as the inlet boundary condition at the cold end, while a symmetric outlet boundary condition is established at the hot end. Conversely, when the gas flows back into the regenerator from the hot end, an inlet boundary condition is enforced at the hot end with the temperature of the heat source, and a symmetric outlet boundary condition is configured at the cold end. To expedite the convergence of the solution process, the temperature of the gas and matrix in the regenerator is initialized with a linear distribution along the axial direction, spanning from the temperature of the cold end to that of the hot end.

$$\dot{m}_{r,cold}=\dot{m}_{kr}, \tag{38}$$

$$p_{r,hot}=p. \tag{39}$$

5.2 Solution procedure

In the present study, the equation systems of the Stirling engine model and the governing equations of the regenerator model are solved using the fourth-order Runge-Kutta method

and the finite volume method, respectively. The detailed solution procedure is illustrated in Figure 4. Firstly, the geometric and operating parameters of the regenerator and engine are given, and the initial conditions of the model are determined on the basis of these specifications. Then the model equation system is solved and the instantaneous physical fields throughout a single cycle are obtained. Thereafter, the temperature and pressure values at the end of the cycle are used to replace the corresponding initial values, and the calculation is repeated until a periodic steady state is achieved. Specifically, if the maximum value of the instantaneous pressure difference between two sequential cycles falls below the threshold of 0.001 MPa, the calculation can be considered to reach a periodic steady state. In the subsequent phase, the ideal power output and heat input of the Stirling engine, as well as the mass flow rate at the cold end of the regenerator and engine pressure, are determined using the steady physical field values.

The mass flow rate and pressure values acquired from the engine model are set as the boundary conditions at the cold and hot ends of the regenerator, respectively. Simultaneously, with the incorporation of these boundary conditions and the specified geometric parameters of the regenerator, the initial conditions can be determined. Subsequently, by solving the governing equations of the regenerator model, the dynamic distributions of different physical variables in the regenerator throughout a cycle are obtained. By replacing the initial values of physical variables with the corresponding values at the end of the cycle, the calculation is carried out several times until the periodic steady state. The criterion for the periodic steady state of the regenerator model is the same as that of the engine model. In the following, the various types of exergy destruction rates in the regenerative process are calculated, and then the ideal power output and heat input of the Stirling engine are corrected by these exergy destruction rates to get the actual power output, thermal efficiency, and exergy efficiency. Throughout these calculations, the time step utilized for both the Stirling engine model and the regenerator model remains consistent at 1/720 of the cycle.

6 Results and discussion

6.1 Model verification

To verify the accuracy of the present mathematical model, a case study is conducted based on the specification parameters of a β-type Stirling engine known as GPU-3, and the numerical results are compared with those from some other thermodynamic models [36,37,58,59], as well as the experimental data obtained from the NASA Lewis Research Center [60]. Table 2 shows the main specifications of the GPU-3 Stirling engine. The comparison of the actual power output P_s among the present model, other thermal models,

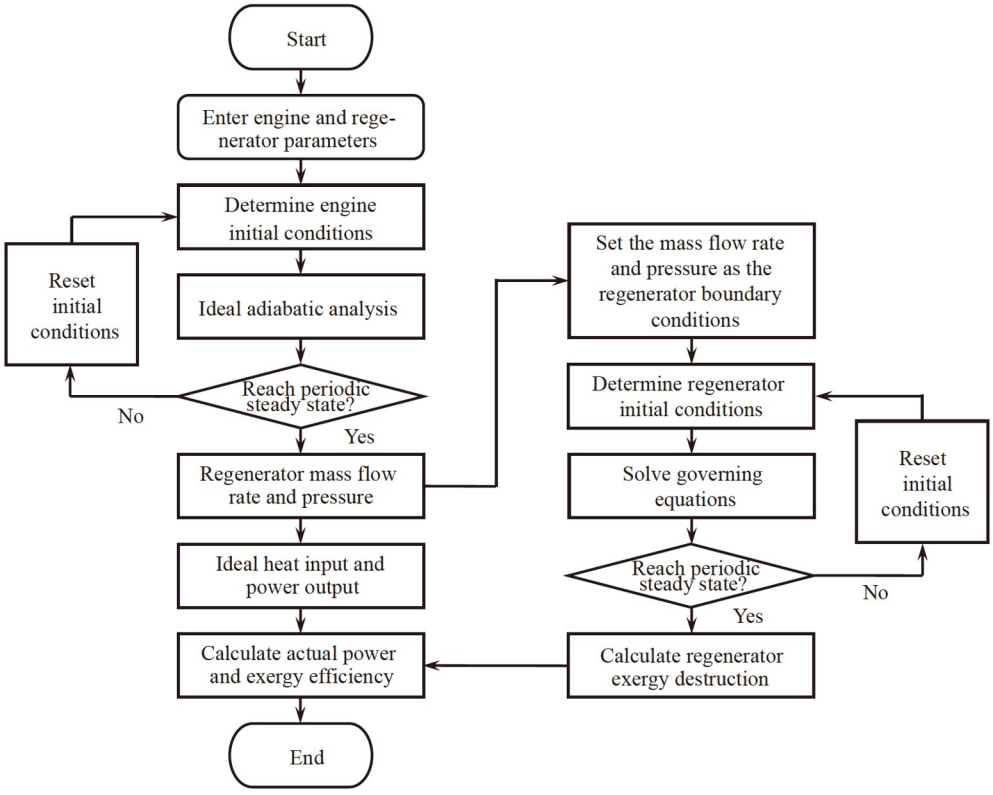

Figure 4 Solution procedure of the Stirling engine and regenerator model.

Table 2 Main specifications of the GPU-3 Stirling engine [24,37,60]

	Specification	Value
General information	Working gas	Helium
	Piston stroke	31.2 mm
	Inner diameter of cylinder	69.9 mm
	Phase angle	90°
	Engine speed	1000–3500 r/min
	Charge pressure	2.76 MPa
Compression chamber	Swept volume	113.14 cm^3
	Clearance volume	28.68 cm^3
General information	Working gas	Helium
	Piston stroke	31.2 mm
Heater	Dead volume	70.88 cm^3
	Heater temperature	922 K
Cooler	Dead volume	13.8 cm^3
	Cooler temperature	288 K
Regenerator	Length	22.6 mm
	Matrix type	Woven screen
	Material	Stainless steel
	Wire diameter	0.04 mm
	Porosity	0.697
	Dead volume	50.55 cm^3

and the experimental work across various engine speeds is illustrated in Figure 5. Notably, the mathematical model presented in this paper exhibits a high degree of accuracy in predicting the impact of regenerators on Stirling engine performance, particularly at relatively high engine speeds. At a low engine speed, the power loss caused by the pressure drop in the regenerator accounts for a minor proportion of the total power losses in Stirling engines, while other power loss factors are not involved in the present model; hence the actual power output predicted by the model exceeds the corresponding experimental results. As the engine speed increases, the regenerator's contribution to the overall pressure drop within the engine proportionally escalates. In turn, the power loss incurred by the regenerators gradually

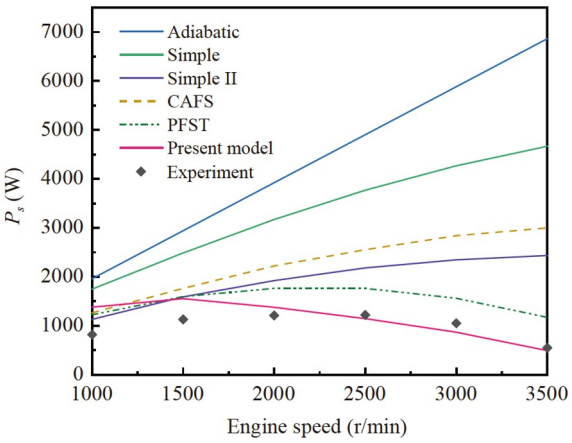

Figure 5 Comparison of the actual power output between the present model and the experimental work at various engine speeds.

approaches the total engine losses. At this juncture, the actual power output calculated by the mathematical model aligns closely with the experimental data, demonstrating a strong agreement.

6.2 Optimization results of matrix structure types

Herein, the heat source temperature is fixed at 973 K, while the engine operates at a constant speed of 1500 r/min. The ranges and initial values of the variables under investigation in this research are listed in Table 3. When analyzing specific variables, unless explicitly stated otherwise, all remaining variables are maintained at their respective initial values. The other specification parameters of the engine adhere to those of the GPU-3 Stirling engine presented in Table 2.

This section performs an optimization analysis of the structure types of the regenerator matrix. Figure 6 shows the effects of the matrix structure coefficient ζ on the regenerator performance. At a low structure coefficient, the geometric characteristics of the inclined-flow regenerator closely resemble those of the parallel-flow regenerator, which leads to a relatively low thermal performance and thus a high heat transfer exergy destruction rate for the inclined-flow regenerator. With the increase of the structure coefficient, the flow resistance of the regenerator rises, but simultaneously, the gas-solid heat transfer rate improves as well. Conse-

Table 3 Ranges and initial values of the variables studied in this work

Variable	Range	Initial value
Total volume of the regenerator V (mm^3)	50000–90000	70000
Structure coefficient of the matrix ζ	0–1	Optimal value
Hydraulic diameter of the matrix d_h (mm)	0.05–1.45	0.25
Porosity of the matrix φ	0.4–0.9	0.7
Length of the regenerator L (mm)	30–100	50

quently, the flow resistance exergy destruction rate increases, while the heat transfer exergy destruction rate decreases significantly, resulting in a decline of the total exergy destruction rate and thus an enhancement of the regenerator performance.

Figure 7 illustrates the impacts of the matrix structure coefficient on the performance of the Stirling engine. When the structure coefficient increases, the engine's actual power output decreases monotonically due to the rising flow resistance exergy destruction rate. However, as observed in Figure 6, the rate of decline in the heat loss and exergy destruction rate caused by heat transfer initially exceeds and then becomes less than the rate of increase in heat loss and exergy destruction rate caused by flow resistance. Consequently, the actual heat and exergy input rate experiences an initial larger reduction followed by a smaller reduction compared to the decrease in actual power output. As a result, both the thermal and exergy efficiency of Stirling engines initially increase, followed by a subsequent reduction. However, there is a slight deviation between the peaks of the thermal efficiency and exergy efficiency. In summary, considering energy utilization efficiency, the engine achieves its best performance within the matrix structure coefficient range of ζ = 0.5–0.6, where it exhibits relatively higher thermal and exergy efficiency. In the subsequent study, the matrix structure coefficient of the regenerator is set to 0.5.

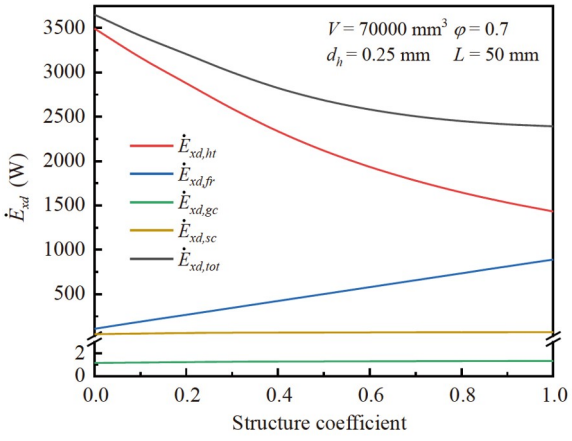

Figure 6 Effects of the matrix structure coefficient on the regenerator performance.

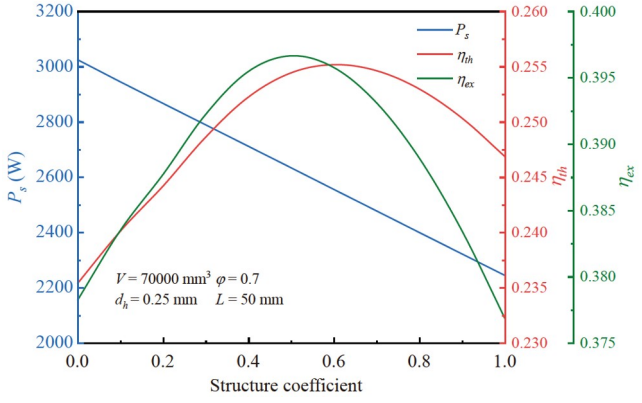

Figure 7 Effects of the matrix structure coefficient on the performance of the Stirling engine.

6.3 Individual contributions to the total exergy destruction rate

Figures 8–10 illustrate the variations in the total exergy destruction rate and its individual contributions to the matrix hydraulic diameter, porosity, and regenerator length, respectively. It is evident from these figures that, under various geometric parameters of regenerators, two types of exergy destruction rates due to axial heat conduction remain relatively low, and the total exergy destruction rate's variability is primarily influenced by the heat transfer and flow resistance exergy destruction rates. In Figure 8, when the hydraulic diameter is small, the regenerator experiences a significant pressure drop due to the presence of very narrow

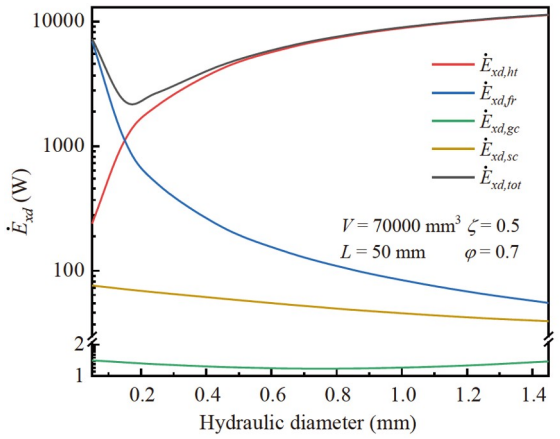

Figure 8 Variations of the total exergy destruction rate and its individual contributions with the matrix hydraulic diameter.

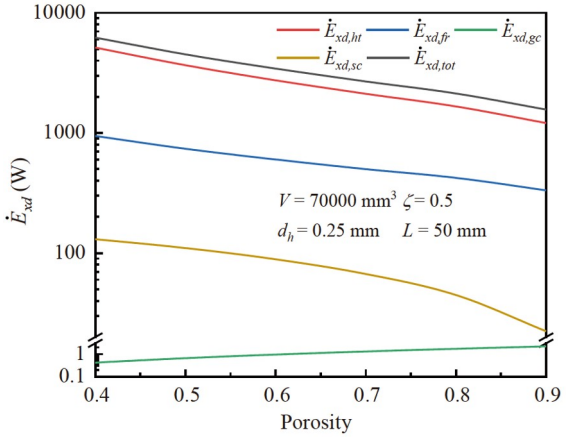

Figure 9 Variations of the total exergy destruction rate and its individual contributions with the matrix porosity.

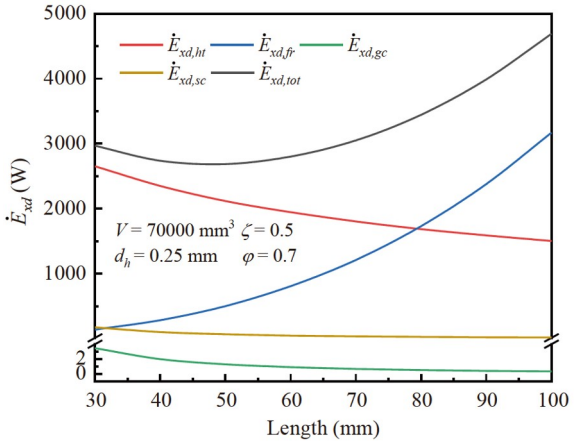

Figure 10 Variations of the total exergy destruction rate and its individual contributions with the regenerator length.

local flow channels. Simultaneously, the matrix's extensive specific surface area contributes to excellent gas-solid heat transfer performance, resulting in a low heat transfer exergy destruction rate. Hence, flow resistance becomes the primary source of exergy destruction in the regenerator. With the increase of the hydraulic diameter, the flow resistance exergy destruction rate decreases substantially, while the heat transfer exergy destruction rate rises rapidly due to the proliferation of microflow channels and a decrease in the specific surface area of the matrix. Consequently, influenced by these opposing changes in exergy destruction rates, the total exergy destruction rate initially decreases and then increases with the hydraulic diameter of the matrix. A minimum total exergy destruction rate is observed at a hydraulic diameter of approximately 0.2 mm.

As depicted in Figure 9, an increase in matrix porosity leads to a weakening of the gas-matrix interaction due to lower gas flow velocity within the matrix. Consequently, the flow resistance exergy destruction rate decreases correspondingly. However, a noteworthy observation is the gradual reduction, rather than an increase, in the heat transfer exergy destruction rate. This phenomenon can be explained by two factors. First, with the rise in porosity, the matrix's specific surface area increases. Second, a longer contact time is available for heat transfer between the gas and the matrix due to the decreased gas flow velocity. These two factors work together to enhance thermal performance and reduce the heat transfer exergy destruction rate. Consequently, as both types of individual exergy destruction rates exhibit similar trends, the total exergy destruction rate consistently decreases with increasing porosity.

As shown in Figure 10, at a low regenerator length, the gas-matrix interaction time is limited. Consequently, gas-solid heat transfer within the regenerator remains insufficient, resulting in a high heat transfer exergy destruction rate. Conversely, a short gas flow distance leads to a low-pressure drop, resulting in a reduced flow resistance exergy destruction rate in the regenerator. As the regenerator length increases, the interaction between the gas and the matrix intensifies, leading to a decrease in the heat transfer exergy destruction rate but an increase in the flow resistance exergy destruction rate. Consequently, the total exergy destruction rate follows a trend of initially decreasing and then increasing, reaching its minimum value at a regenerator length of approximately 45 mm.

6.4 Sensitive analyses for regenerator geometries

Analyses of the regenerator characteristics and Stirling engine performance concerning the matrix hydraulic diameter, porosity, and regenerator length, considering variable total volumes of regenerators, are presented in Figures 11–13. Figure 11 illustrates that under different total volumes of regenerators, the total exergy destruction rate reaches its minimum value at a hydraulic diameter of approximately 0.2 mm. Deviations from this range, whether smaller or larger hydraulic diameters, can result in reduced overall regenerator performance due to increased exergy destruction in flow resistance or heat transfer. Notably, for regenerators with hydraulic diameters d_h less than 0.05 mm, excessive pressure loss within the regenerator causes Stirling engines to malfunction, yielding actual power output, thermal efficiency, and exergy efficiency all below 0. As hydraulic diameter increases beyond 0.2 mm, the actual power output of Stirling engines experiences a rapid increase, leading to a substantial boost in both thermal and exergy efficiency. However, when the hydraulic diameter surpasses 0.2 mm, the actual power output stabilizes, while engine heat and exergy input increase significantly due to higher thermal losses in the regenerator. Consequently, thermal and exergy efficiency are reduced.

In addition, an increase in regenerator volume leads to an expanded cross-sectional area within the regenerator, resulting in decreased gas flow velocity within the matrix. Consequently, the flow resistance exergy destruction rate decreases. Simultaneously, the enlarged effective heat transfer area and extended interaction time between the gas and matrix reduce the heat transfer exergy destruction rate. This combined effect results in a reduction in the total exergy destruction rate of the regenerator with an increasing regenerator volume. Moreover, for the regenerator with a larger total volume, both the ideal power output and power loss due to the flow resistance in the regenerator decrease. When the matrix hydraulic diameter $d_h < 0.45$ mm, the reduction in flow resistance exergy destruction rate is more significant than the decrease in ideal power output, leading to an increase in actual power output as the regenerator volume rises. However, for d_h values greater than 0.45 mm, this trend is reversed. On the other hand, as the variation of the thermal

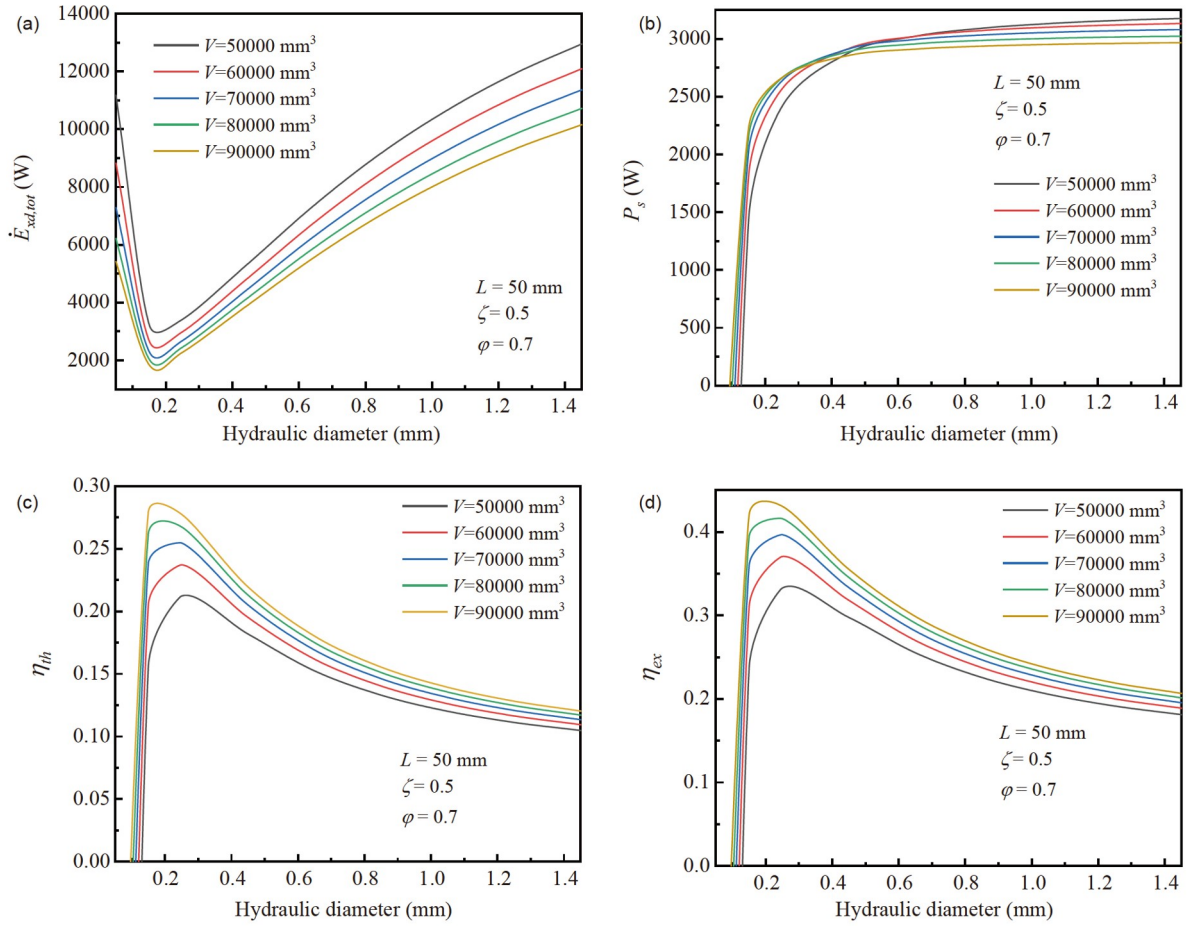

Figure 11 Effects of the matrix hydraulic diameter on the comprehensive performance of the regenerator and Stirling engine under variable regenerator volumes.

loss and heat transfer exergy destruction rate is more pronounced than that of the actual power output, the thermal and exergy efficiency of the engine increases with an expanding regenerator volume.

Under various regenerator volumes, the comprehensive performance of the regenerator is improved with an increase in matrix porosity, as depicted in Figure 12. As porosity increases, the ideal power output of the engine experiences a slight decline due to the larger dead volume within the regenerator. Concurrently, the flow resistance exergy destruction rate decreases with increasing porosity, but the extent of this reduction is notably influenced by the regenerator volume. Specifically, for regenerators with smaller total volumes, a higher porosity is crucial for achieving a low flow resistance exergy destruction rate and thus a high actual power output of the engine. However, for regenerators with larger volumes, the reduction in flow resistance loss is relatively modest. This leads to a gradual increase in actual power output at low porosities and even a decrease at high porosities. Due to the decreasing thermal loss and heat transfer exergy destruction rate, combined with a general increase in power output, the energy and exergy efficiency of the engine consistently rises with increasing porosity. These results suggest that a regenerator with higher porosity is necessary to attain superior regenerator and Stirling engine performance. However, it is important to note that in this study, the ideal Stirling engine performance is determined under the assumption of perfect regeneration, without considering the impact of the regenerator's thermal mass ratio on regenerative effectiveness. In reality, achieving a sufficiently high thermal mass ratio is critical to ensure effective regeneration in the regenerator. This implies that the regenerator matrix should not possess an excessively high porosity.

According to the results in Figure 13, the total exergy destruction rate of the regenerator exhibits a slight initial decrease followed by an increase as the regenerator length varies under different regenerator volumes. Simultaneously, the engine with a longer regenerator yields a lower actual power output, primarily due to the elevated flow resistance exergy destruction rate within the regenerator. Considering the observed trends in thermal loss, heat transfer exergy destruction rate, and actual power output, the overall energy and exergy efficiency of the engine follow a general

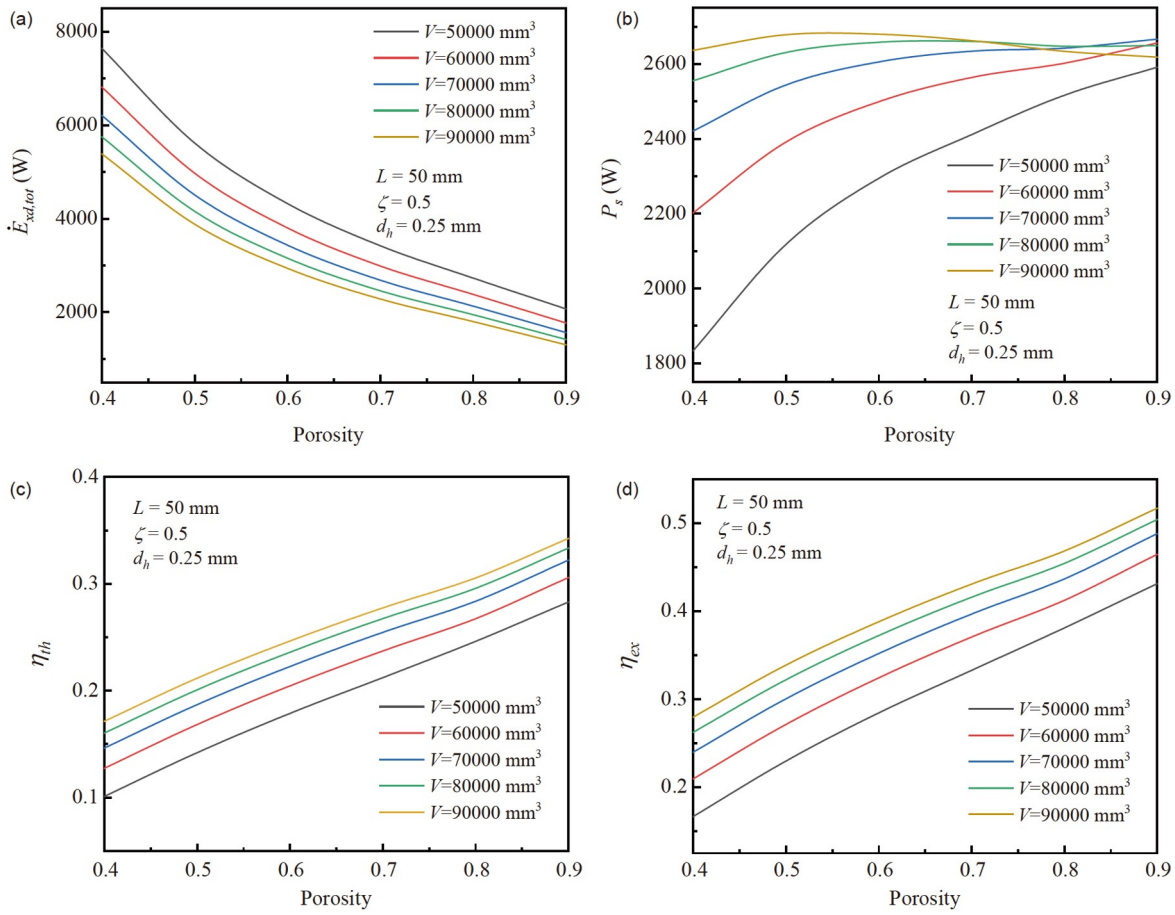

Figure 12 Effects of the matrix porosity on the comprehensive performance of the regenerator and Stirling engine under variable regenerator volumes.

tendency of decline. It is noteworthy that the gas flow velocity within the regenerator experiences more pronounced changes in response to variations in regenerator length under smaller regenerator volumes compared to larger ones. This leads to a more sensitive impact on the performance of both the regenerator and the Stirling engine as regenerator length changes. Additionally, a comprehensive analysis of Figures 11–13 reveals that, regardless of matrix hydraulic diameter, porosity, or regenerator length, the overall performance of the regenerator and the engine improves with increasing regenerator volume. Nevertheless, the total volume of the regenerator cannot be infinitely increased, as it is constrained by the global assembly layout and manufacturing costs of the Stirling engine.

7 Conclusions

By integrating the ideal adiabatic Stirling model with a one-dimensional regenerator mathematical model, a relationship between regenerator structure and Stirling engine behavior was established to achieve superior engine performance by selecting an optimal regenerator. To achieve an excellent overall thermo-hydraulic characteristic, a new concept of inclined-flow regenerators with the matrix surface inclined to the gas flow direction was proposed. An energy and exergy analysis was conducted at the engine level to provide insights for selecting regenerator structures that minimize regenerator exergy destruction while maximizing engine power output, thermal efficiency, and exergy efficiency. Several key findings are summarized as follows.

(1) Increasing the matrix structure coefficient results in a consistent decrease in the actual power output of Stirling engines. Conversely, energy and exergy efficiency show an initial rise followed by a decline, with peak values occurring at structure coefficients of 0.5 and 0.6, respectively. Consequently, for optimized energy utilization efficiency, Stirling engines equipped with inclined-flow regenerators exhibiting structural and thermo-hydraulic characteristics between cross-flow and parallel-flow regenerators demonstrate superior performance. Herein, a structure coefficient of 0.5 is selected for the structural optimization of inclined-flow regenerators. Subsequent to this study, specific structural designs for inclined-flow regenerators will be implemented for practical application.

(2) Due to the minimal axial heat conduction losses within

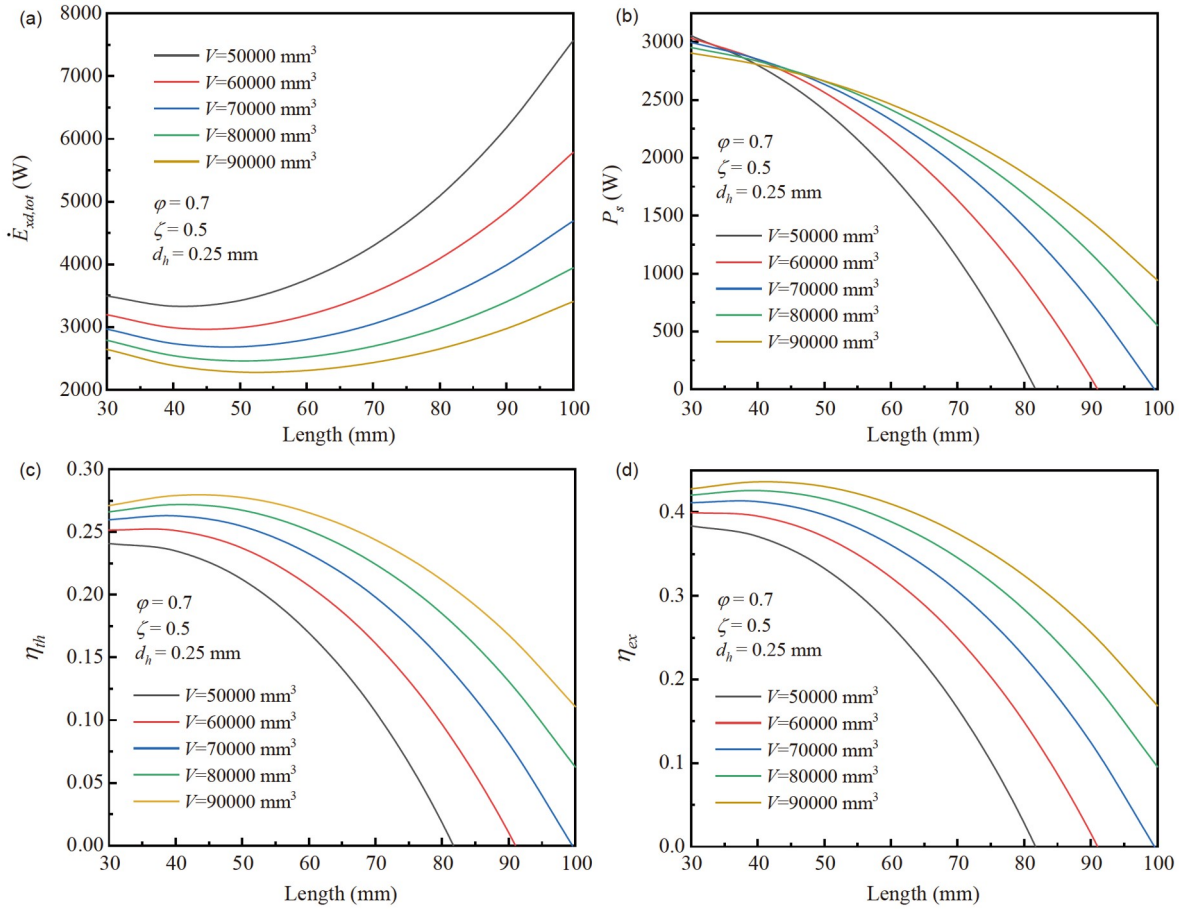

Figure 13 Effects of the regenerator length on the comprehensive performance of the regenerator and Stirling engine under variable regenerator volumes.

the gas and matrix, the total exergy destruction rate within the regenerator is primarily dictated by the individual exergy destruction rates arising from gas-solid heat transfer with finite temperature differences and gas flow resistance. As the matrix hydraulic diameter and regenerator length increase, a minimum total exergy destruction rate is achieved due to the opposing variations in the heat transfer and flow resistance exergy destruction rates under specific values of these geometric parameters. Conversely, greater matrix porosity results in diminished contributions to the individual exergy destruction rates, leading to a reduction in the overall exergy destruction rate.

(3) With the increase of the local geometric parameters including the matrix hydraulic diameter and regenerator length, regenerator performance initially improves and then declines. This implies the existence of optimal hydraulic diameter and regenerator length values that result in the lowest exergy destruction in regenerators. Conversely, when global geometric parameters like matrix porosity and total regenerator volume are increased, regenerator performance can be enhanced due to reduced pressure loss and prolonged heat transfer duration within the regenerator.

(4) The actual power output increases with an increase in matrix hydraulic diameter, porosity, and regenerator volume, and a decrease in regenerator length overall. On the other hand, the engine's energy and exergy efficiency improve as porosity and regenerator volume increase and as regenerator length decreases. However, as the matrix hydraulic diameter increases, there is an initial rapid increase in energy utilization efficiency followed by a subsequent decrease. Following structural optimization, Stirling engines equipped with inclined-flow regenerators exhibit significant improvements compared to cross-flow regenerators, with a 16.6% increase in output power and a substantial 38.7% and 37.2% boost in thermal and exergy efficiency, respectively. In comparison to parallel-flow regenerators, they experience a 13.5% reduction in output power but achieve notable enhancements of 45.4% and 36.7% in thermal and exergy efficiency, respectively.

This work was supported by the National Natural Science Foundation of China (Grant No. 51736004).

1 Liu Y, Xiao L Y, Wang H F, et al. Analysis on the hourly spatio-temporal complementarities between China's solar and wind energy resources spreading in a wide area. Sci China Tech Sci, 2013, 56: 683–692

2 Wu H F, Zhang B W, Qu W J, et al. Integration of a thermochemical energy system driven by solar energy and biomass for natural gas and power production. Sci China Tech Sci, 2022, 65: 1383–1395
3 Wang K, Sanders S R, Dubey S, et al. Stirling cycle engines for recovering low and moderate temperature heat: A review. Renew Sustain Energy Rev, 2016, 62: 89–108
4 Zhou B, Cheng X T, Liang X G. Power output analyses and optimizations of the Stirling cycle. Sci China Tech Sci, 2013, 56: 228–236
5 Chen W L, Wong K L, Chang Y F. A numerical study on the effects of moving regenerator to the performance of a β-type Stirling engine. Int J Heat Mass Transfer, 2015, 83: 499–508
6 Liu M, Zhang B, Han D, et al. Experimental study on regenerative effectiveness and flow characteristics of parallel-plate regenerator in Stirling engine. Appl Thermal Eng, 2022, 217: 119139
7 Costa S C, Barreno I, Tutar M, et al. The thermal non-equilibrium porous media modelling for CFD study of woven wire matrix of a Stirling regenerator. Energy Convers Manage, 2015, 89: 473–483
8 Srinivasan K V, Manimaran A, Arulprakasajothi M, et al. Design and development of porous regenerator for Stirling cryocooler using additive manufacturing. Thermal Sci Eng Prog, 2019, 11: 195–203
9 Alfarawi S, AL-Dadah R, Mahmoud S. Transient investigation of mini-channel regenerative heat exchangers: Combined experimental and CFD approach. Appl Thermal Eng, 2017, 125: 346–358
10 Kato Y. Indicated diagrams of low temperature differential Stirling engines with channel-shaped heat exchangers. Renew Energy, 2017, 103: 30–37
11 Chen W L, Wong K L, Chen H E. An experimental study on the performance of the moving regenerator for a γ-type twin power piston Stirling engine. Energy Convers Manage, 2014, 77: 118–128
12 Gedeon D, Wood J G. Oscillating-flow regenerator test rig: Hardware and theory with derived correlations for screens and felts. NASA CR-198442, 1996. 6–13
13 de Monte F, Rosa P. Linear analysis of rapidly switched heat regenerators in counterflow. Int J Heat Mass Transfer, 2008, 51: 3642–3655
14 Costa S C, Barrutia H, Esnaola J A, et al. Numerical study of the heat transfer in wound woven wire matrix of a Stirling regenerator. Energy Convers Manage, 2014, 79: 255–264
15 Yu Z, Mao X, Jaworski A J. Experimental study of heat transfer in oscillatory gas flow inside a parallel-plate channel with imposed axial temperature gradient. Int J Heat Mass Transfer, 2014, 77: 1023–1032
16 Costa S C, Barrutia H, Esnaola J A, et al. Numerical study of the pressure drop phenomena in wound woven wire matrix of a Stirling regenerator. Energy Convers Manage, 2013, 67: 57–65
17 Ni M, Peng H, Sultan U, et al. A quantitative method to describe the flow characteristics of an oscillating flow including porous media. Int J Heat Mass Transfer, 2018, 119: 860–866
18 Xiao G, Peng H, Fan H, et al. Characteristics of steady and oscillating flows through regenerator. Int J Heat Mass Transfer, 2017, 108: 309–321
19 Yanaga K, Li R, Qiu S. Robust foil regenerator flow loss and heat transfer tests under oscillating flow condition. Appl Thermal Eng, 2020, 178: 115525
20 Gheith R, Aloui F, Ben Nasrallah S. Study of temperature distribution in a Stirling engine regenerator. Energy Convers Manage, 2014, 88: 962–972
21 Kato Y, Baba K. Empirical estimation of regenerator efficiency for a low temperature differential Stirling engine. Renew Energy, 2014, 62: 285–292
22 Dai D D, Yuan F, Long R, et al. Imperfect regeneration analysis of Stirling engine caused by temperature differences in regenerator. Energy Convers Manage, 2018, 158: 60–69
23 Ahmadi M H, Mohammadi A H, Dehghani S, et al. Multi-objective thermodynamic-based optimization of output power of Solar Dish-Stirling engine by implementing an evolutionary algorithm. Energy Convers Manage, 2013, 75: 438–445
24 Chahartaghi M, Sheykhi M. Energy and exergy analyses of beta-type Stirling engine at different working conditions. Energy Convers Manage, 2018, 169: 279–290
25 Li R, Grosu L, Queiros-Condé D. Losses effect on the performance of a Gamma type Stirling engine. Energy Convers Manage, 2016, 114: 28–37
26 Cheng C H, Yang H S, Keong L. Theoretical and experimental study of a 300-W beta-type Stirling engine. Energy, 2013, 59: 590–599
27 Nielsen A S, York B T, MacDonald B D. Stirling engine regenerators: How to attain over 95% regenerator effectiveness with sub-regenerators and thermal mass ratios. Appl Energy, 2019, 253: 113557
28 Ahmadi M H, Hosseinzade H, Sayyaadi H, et al. Application of the multi-objective optimization method for designing a powered Stirling heat engine: Design with maximized power, thermal efficiency and minimized pressure loss. Renew Energy, 2013, 60: 313–322
29 Cheng C H, Yu Y J. Numerical model for predicting thermodynamic cycle and thermal efficiency of a beta-type Stirling engine with rhombic-drive mechanism. Renew Energy, 2010, 35: 2590–2601
30 Kato Y, Saitoh S, Ishimatsu K, et al. Effect of geometry and speed on the temperatures estimated by CFD for an isothermal model of a gamma configuration low temperature differential Stirling engine with flat-shaped heat exchangers. Appl Thermal Eng, 2017, 115: 111–122
31 Gheith R, Aloui F, Ben Nasrallah S. Determination of adequate regenerator for a Gamma-type Stirling engine. Appl Energy, 2015, 139: 272–280
32 Kongtragool B, Wongwises S. A review of solar-powered Stirling engines and low temperature differential Stirling engines. Renew Sustain Energy Rev, 2003, 7: 131–154
33 Kongtragool B, Wongwises S. Investigation on power output of the gamma-configuration low temperature differential Stirling engines. Renew Energy, 2005, 30: 465–476
34 Ahmadi M H, Ahmadi M A, Pourfayaz F, et al. Optimization of powered Stirling heat engine with finite speed thermodynamics. Energy Convers Manage, 2016, 108: 96–105
35 Dai D, Liu Z, Yuan F, et al. Finite time thermodynamic analysis of a solar duplex Stirling refrigerator. Appl Thermal Eng, 2019, 156: 597–605
36 Urieli I, Berchowitz D M. Stirling Cycle Engine Analysis. Bristol: Adam Hilger Ltd., 1984
37 Babaelahi M, Sayyaadi H. Simple-II: A new numerical thermal model for predicting thermal performance of Stirling engines. Energy, 2014, 69: 873–890
38 Ni M, Shi B, Xiao G, et al. Improved simple analytical model and experimental study of a 100 W β-type Stirling engine. Appl Energy, 2016, 169: 768–787
39 Babaelahi M, Sayyaadi H. A new thermal model based on polytropic numerical simulation of Stirling engines. Appl Energy, 2015, 141: 143–159
40 Li R, Grosu L, Li W. New polytropic model to predict the performance of beta and gamma type Stirling engine. Energy, 2017, 128: 62–76
41 Babaelahi M, Sayyaadi H. Modified PSVL: A second order model for thermal simulation of Stirling engines based on convective-polytropic heat transfer of working spaces. Appl Thermal Eng, 2015, 85: 340–355
42 Wang K, Dubey S, Choo F H, et al. A transient one-dimensional numerical model for kinetic Stirling engine. Appl Energy, 2016, 183: 775–790
43 Qiu H, Wang K, Yu P, et al. A third-order numerical model and transient characterization of a β-type Stirling engine. Energy, 2021, 222: 119973
44 de la Bat B J G, Harms T M, Dobson R T, et al. Derivation and numerical case study of a one-dimensional, compressible-flow model of a novel free-piston Stirling engine. Energy, 2020, 199: 117404
45 Alfarawi S, AL-Dadah R, Mahmoud S. Influence of phase angle and dead volume on gamma-type Stirling engine power using CFD simulation. Energy Convers Manage, 2016, 124: 130–140
46 Abuelyamen A, Ben-Mansour R, Abualhamayel H, et al. Parametric

study on beta-type Stirling engine. Energy Convers Manage, 2017, 145: 53–63
47 Chen W L, Yang Y C, Salazar J L. A CFD parametric study on the performance of a low-temperature-differential γ-type Stirling engine. Energy Convers Manage, 2015, 106: 635–643
48 Xiao G, Sultan U, Ni M, et al. Design optimization with computational fluid dynamic analysis of β-type Stirling engine. Appl Thermal Eng, 2017, 113: 87–102
49 Zare S, Tavakolpour-saleh A R, Aghahosseini A, et al. Design and optimization of Stirling engines using soft computing methods: A review. Appl Energy, 2021, 283: 116258
50 Xu H J, Xing Z B, Wang F Q, et al. Review on heat conduction, heat convection, thermal radiation and phase change heat transfer of nanofluids in porous media: Fundamentals and applications. Chem Eng Sci, 2019, 195: 462–483
51 Trevizoli P V, Barbosa Jr. J R. Entropy generation minimization analysis of oscillating-flow regenerators. Int J Heat Mass Transfer, 2015, 87: 347–358
52 Tanaka M, Yamashita I, Chisaka F. Flow and heat transfer characteristics of the stirling engine regenerator in an oscillating flow. JSME Int J, 1990, 33: 283–289
53 Alfarawi S, AL-Dadah R, Mahmoud S. Potentiality of new miniature-channels Stirling regenerator. Energy Convers Manage, 2017, 133: 264–274
54 Yu M, Xin F, Lai X, et al. Study of oscillating flows through a novel constructal bifurcation Stirling regenerator. Appl Thermal Eng, 2021, 184: 116413
55 Wang J B, Liu Z C, Liu W. Evaluation of convective heat transfer in a tube based on local exergy destruction rate. Sci China Tech Sci, 2016, 59: 1494–1506
56 Zhang X R, Li X J. Energy and exergy performance investigation of transcritical CO_2-based Rankine cycle powered by solar energy. Sci China Tech Sci, 2012, 55: 1427–1436
57 Li P L, Chen L G, Xia S J, et al. Total entropy generation rate minimization configuration of a membrane reactor of methanol synthesis via carbon dioxide hydrogenation. Sci China Tech Sci, 2022, 65: 657–678
58 Hosseinzade H, Sayyaadi H. CAFS: The combined adiabatic-finite speed thermal model for simulation and optimization of Stirling engines. Energy Convers Manage, 2015, 91: 32–53
59 Hosseinzade H, Sayyaadi H, Babaelahi M. A new closed-form analytical thermal model for simulating Stirling engines based on polytropic-finite speed thermodynamics. Energy Convers Manage, 2015, 90: 395–408
60 Martini W R. Stirling engine design manual. Technical Report. Richland: Martini Engineering, 1983